Journal of Materials Chemistry B

PAPER

View Article Online
View Journal | View Issue

Cite this: J. Mater. Chem. B, 2018, 6, 2584

Mannan-based conjugates as a multimodal imaging platform for lymph nodes†

M. Rabyk,[a] A. Galisova,[b] M. Jiratova,[b] V. Patsula,[a] L. Srbova,[a] L. Loukotova,[a] J. Parnica,[a] D. Jirak,[b] P. Stepanek[a] and M. Hruby *[a]

Received 6th November 2017,
Accepted 3rd January 2018

DOI: 10.1039/c7tb02888a

rsc.li/materials-b

We show that mannan-based conjugates possess exceptional features for multimodal imaging because of their biocompatibility, biodegradability and self-targeting properties. Two new mannan conjugates, containing a gadolinium complex and a fluorescent probe, one based only on polysaccharide and the other one comprising polysaccharide with poly(2-methyl-2-oxazoline) grafts, were prepared and simultaneously visualized *in vitro* and *in vivo* by magnetic resonance and fluorescence imaging. The synthesis of these mannan-based complexes was based on alkylation with allyl bromide or grafting with poly(2-methyl-2-oxazoline) chains, followed by a thiol–ene click reaction with cysteamine to introduce primary amino groups into their structure. Finally, the obtained conjugates were functionalized with contrast labels using the corresponding *N*-hydroxysuccinimide esters. When used to detect lymph nodes, the polymers showed better imaging properties than a commercially available contrast agent.

Introduction

Recently, the usage of polysaccharides for pharmaceutical and biomedical applications has been the subject of numerous studies[1,2] because of their unique physicochemical and biological properties.[3,4] Polysaccharides may serve as carriers suitable for the construction of delivery systems for drugs,[5–7] as vaccine adjuvants,[8] as components of designed gene delivery systems[9] and tissue engineering scaffolds,[10–12] *etc.* Such carbohydrate-based systems are often produced by polyelectrolyte complexation,[13] covalent chemical modification of the polysaccharide;[14] chemical crosslinking[15] or grafting with a synthetic polymer.[16]

Polysaccharides may also be used for the preparation of diagnostic probes.[17–19] Although most of the studies conducted in this biomedical field are dedicated to cancer diagnostics, there is also a need to investigate methods for detecting possible complications related to cancer. One of these complex issues connected with cancer is the detection of sentinel lymph nodes (SLNs). As part of immune system, lymph nodes (LNs) play a very important role in the body. Among other types of cells, they include B- and T-lymphocytes, which monitor lymph for the presence of ''foreign'' bacteria and viruses; when such objects are detected, they become activated by migratory dendritic cells (DC), and an immune response is subsequently triggered.[20]

LNs also play a key role in metastatic process. Although the mechanism is not absolutely clear yet, it is well know that because of the large cavity of lymph vessels and slow velocity of lymph itself, the lymphatic system possesses a huge capacity for tumour metastasis. Many types of malignant tumours, such as melanoma and breast and prostate cancers, are prone to metastasize to the regional LNs through the tumour-associated lymphatic vessels.[21] Consequently, the LN nearest to where cancer cells are spread to from a primary tumour is called the SLN. Currently, the typical procedure for SLN diagnosis is biopsy (SLNB)[22] with subsequent pathological analysis, which is based on immunohistochemical staining with cytokeratin 19 (CK19).[23] Although SLNB is less burdensome for patients than axillary lymph node dissection, it still possesses all the drawbacks associated with any surgery.[24–27] Nevertheless, the clinical advantage of SLNB over node dissection is unquestionable, and the procedure has become the favoured choice for patients with breast cancer, melanoma, and colorectal and prostate cancers.[28,29] A few studies using magnetic resonance imaging (MRI) for cancer diagnosis and LN visualization were reported,[30,31] showing a considerable potential of the method. However, this technique remains an additional diagnostic tool rather than a primary one, and deeper research in the field is justified. Additionally, a few other works have promoted SLNs investigation using combined methods, for instance, with the single-photon emission computed tomography (SPECT)/MRI[32] and positron emission tomography (PET)/near infrared fluorescence (NIRF)[33] techniques. The available methods and materials

[a] Institute of Macromolecular Chemistry, Academy of Sciences of the Czech Republic, Prague, Czech Republic. E-mail: mhruby@centrum.cz
[b] Institute for Clinical and Experimental Medicine, Czech Republic

† Electronic supplementary information (ESI) available. See DOI: 10.1039/c7tb02888a

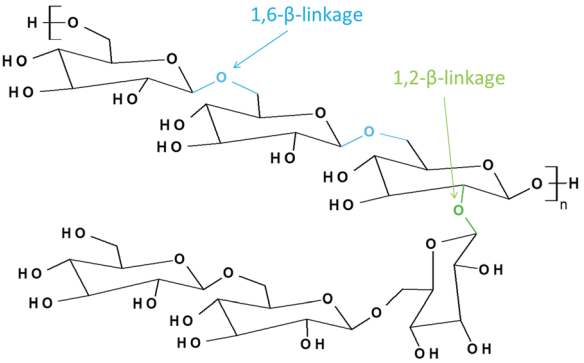

Scheme 1 Chemical structure of native mannan from *Saccharomyces cerevisiae*.

used for these purposes were nicely and thoroughly reviewed elsewhere.[34,35] Undoubtedly, the development of new prospective methodology and materials for use in SLN diagnostics is currently essential.

The useful biological properties of mannan (MN) inspired us to use it as a platform for preparing new multimodal probes. For this work, commercially available MN from *Saccharomyces cerevisiae* was selected, which consists of an α-1,6-linked mannose backbone with a high percentage of α-1,2 and α-1,3 side chains of different compositions[36] (Scheme 1). MN is biocompatible, biodegradable, and nontoxic, and due to the presence of numerous hydroxyl groups in its structure, it can easily be modified to achieve the desired properties. These characteristics all make MN a promising candidate for the development of new polysaccharide-based nanocarriers for biomedical applications.

In a living organism, MN binds to the mannose receptors, which are a class of multilectin receptor proteins that provide a link between innate and adaptive immunity.[37] Consequently, MN is preferably accumulated in immune cells[38] overexpressing the DC-SIGN receptors (dendritic cell-specific ICAM-grabbing non-integrin receptors, where ICAM is intracellular adhesion molecule), which could be useful for detecting SLNs and inflammations, which are heavily infiltrated with macrophages and DCs. This raises the possibility of using MN as a probe for investigating pathological processes and developing corresponding therapies.

In the past few decades, numerous works have contributed to the synthesis and characterization of poly(2-alkyl-2-oxazoline)s as perspective materials for biomedical applications.[39–42] The reason for such high interest lies in the biocompatibility and non-toxicity of these bio-inspired polymers along with the wide variety of accessible properties, which depend on the structure and can be easily tailored during synthesis or by a post-modification procedure. Thus, the aim of this study was preparing new hybrid polymer contrast agents based on MN intended for detecting of SLNs by multimodal imaging. We designed and critically compared two new MN-based conjugates: one based only on polysaccharide and the other one comprasing polysaccharide with poly(2-methyl-2-oxazoline) (POX) grafts. Both conjugates contained a gadolinium complex and a fluorescent probe for the magnetic resonance imaging (MRI) and optical fluorescence imaging (FLI) modalities, respectively. These conjugates were simultaneously visualized *in vitro* and *in vivo* by MRI and FLI; moreover, the accumulation of the conjugates in LNs was also shown. Grafting with POX was performed to slow down biodegradation and therefore prolong the diagnostic window for imaging. Both MN-based contrast agents were compared with clinically used gadoterate meglumine (GM) in an *in vitro*/*in vivo* animal model, showing the striking potential of our probes for LN detection.

Experimental part

Materials

Mannan (MN) from *Saccharomyces cerevisiae*, 2-methyl-2-oxazoline and gadolinium(III) chloride (anhydrous) were purchased from Sigma-Aldrich Ltd (Prague, Czech Republic). Diethyl ether, dimethyl sulfoxide (DMSO), sodium chloride and toluene were purchased from Lachner Ltd (Neratovice, Czech Republic). 1,4,7,10-Tetraazacyclododecane-1,4,7,10-tetraacetic acid *N*-hydroxysuccinimide ester (DOTA-NHS-ester) was purchased from Macrocyclics, Inc. (Plano, USA). IR800CW-NHS-ester was purchased from LI-COR Biotechnology – GmbH (Bad Homburg, Germany). 2,4,6-Trinitrobenzene-1-sulfonic acid (TNBSA) solution was purchased from Thermo Fisher Scientific (Praha, Czech Republic). Ultrapure Q-water ultrafiltered with a Milli-Q Gradient A10 system (Millipore, Molsheim, France) was used throughout the work. Spectra/Por dialysis membranes (molecular weight cut-offs (MWCOs) of 3.5×10^3 and 6–8 $\times 10^3$ g mol^{-1}) were purchased from P-LAB (Prague, Czech Republic). All other chemicals were purchased from Sigma-Aldrich Ltd (Prague, Czech Republic) and were used without further purification unless stated otherwise.

Synthesis and preparation

Preparation of allylated mannan (MN_allyl). MN from *S. cerevisiae* (0.6 g, 3.7 mmol glucose units) and sodium hydroxide (0.296 g, 7.4 mmol) were dissolved in water (22 mL), and the solution was cooled to 0 °C. Allyl bromide (100 μL, 1.16 mmol) was added, and the mixture was stirred for 10 h at 0 °C and then overnight at room temperature. Acetic acid (0.65 mL, 11.4 mmol) was added to neutralize the residual sodium hydroxide; the resulting solution was dialyzed against water using Spectra/Por 3 membrane tubing with a MWCO of 3500 g mol^{-1} for 48 h and freeze-dried. Yield: 0.597 g (99%) of allylated mannan (MN_allyl, 12.66 mol%).

^{1}H-NMR of MN_allyl (300 MHz, D_2O), δ (ppm): 3.5–4.2 (–C**H**$_2$–CH–, mannose; C**H**$_2$═CH–C**H**$_2$–), 4.9–5.3 (–O–C**H**–O, acetal), 5.95 (CH$_2$═C**H**–).

Preparation of mannan-*graft*-poly(2-methyl-2-oxazoline) with theoretical molecular weight of grafts $M_{n,graft}$ = 1000 g mol^{-1} (synthesis of MN_POX). 2-Methyl-2-oxazoline (1.5 mL, 17.71 mmol) and allyl bromide (0.259 mL, 2.99 mmol) were mixed with 7 mL of anhydrous acetonitrile, and the reaction mixture was stirred overnight at 70 °C under an argon atmosphere. MN from *S. cerevisiae* (1 g, 6.17 mmol of glucose units) was dissolved in 23 mL of anhydrous DMSO and the solution was azeotropically

dried by multiple additions of anhydrous toluene (5 mL) and subsequent evaporation at 70 °C under reduced pressure. Sodium hydride (1.7 g of a 60% dispersion in mineral oil, 42.5 mmol) was added to the MN solution, and the mixture was stirred for 3 h at 70 °C. The poly(2-methyl-2-oxazoline) (POX) polymerization mixture (6.86 g) was added to solution of MN sodium alkoxide in DMSO, and the resulting mixture was stirred overnight at 70 °C. Water (10 mL) was added to the reaction mixture, and the resulting suspension was washed twice with diethyl ether (~50 mL) to remove the mineral oil. Finally, the aqueous layer was dialyzed (MWCO of 6–8 × 10^3 g mol^{-1}) against water for 72 h and freeze-dried to provide the desired product, mannan-*graft*-poly(2-methyl-2-oxazoline) (MN_POX, 0.943 g, 94.25% yield). The remaining 0.65 mL of POX solution was mixed with 0.25 mL water and purified on a Sephadex® LH-20 column using methanol as the mobile phase and evaporated to obtain only the corresponding polymer grafts terminated with –OH groups.

^{1}H-NMR of POX grafts (300 MHz, CD_3OD), δ (ppm): 2.04 (–C**H**$_3$), 3.5–4.3 (–N–C**H**$_2$–C**H**$_2$–, C**H**$_2$═CH–), 5.85 (CH_2═C**H**–). Matrix-assisted laser desorption/ionization (MALDI) mass spectrometry of POX grafts: M_n = 870 g mol^{-1}, I = 1.14. ^{1}H-NMR of MN_POX (300 MHz, D_2O), δ (ppm): 1.99 (–C**H**$_3$, POX), 3.5–4.2 (–C**H**$_2$–C**H**–, mannose; –N–C**H**$_2$–C**H**$_2$–, POX; C**H**$_2$═CH–), 4.99–5.24 (–O–C**H**–O, acetal), 5.9 (CH_2═C**H**–). Elemental analysis of MN_POX: C 41.83%, H 7.13%, N 3.28%.

Addition of cysteamine to MN_allyl or MN_POX (synthesis of MN_NH$_2$ or MN_POX_NH$_2$). The product MN_allyl (0.612 g, 0.489 mmol) or MN_POX (0.834 g, 1.029 mmol), cysteamine (0.616 g, 7.98 mmol or 0.836 g, 10.84 mmol for MN_allyl and MN_POX, respectively) and hydrochloric acid (36%, 649 μL, 7.96 mmol or 886.5 μL, 10.87 mmol for MN_allyl and MN_POX, respectively) were dissolved in 13 mL or 17 mL of distilled water (for MN_allyl and MN_POX, respectively) and cooled to 0 °C. A solution of 2-hydroxy-2-methylpropiophenone in ethanol (0.33 vol%, 490 μL or 667 μL for MN_allyl and MN_POX, respectively) was added, and the reaction mixture was irradiated by a UV lamp (TESLA RVK 6 × 125 W) for 60 min. Then, a solution of sodium carbonate (10 wt%, 30.75 mL or 41.69 mL for MN_allyl and MN_POX, respectively) was added, and the aqueous layer was washed with diethyl ether (~20 mL), dialyzed (MWCO 3.5 × 10^3 g mol^{-1}) against water for 48 h and freeze-dried. The resulting products were purified on a Sephadex® G-25 column using water as the mobile phase and freeze-dried to afford the products MN_NH$_2$ and MN_POX_NH$_2$ (514 mg and 689 mg, respectively). The content of –NH_2 groups was determined by their specific reaction[43] with TNBSA, which provided a soluble coloured product that was determined spectrophotometrically (0.236 mmol g^{-1} and 0.195 mmol g^{-1} of –NH_2 groups for MN_NH$_2$ and MN_POX_NH$_2$, respectively).

^{1}H-NMR of MN_NH$_2$ (600 MHz, DMSO), δ (ppm): 2.64 (–S–CH_2–C**H**$_2$–NH_2), 2.8 (–S–C**H**$_2$–CH_2–NH_2), 3.4–4.2 (–C**H**$_2$–C**H**–, mannose; C**H**$_2$═CH–), 4.9–5.2 (–O–C**H**–O, acetal), 5.92 (CH_2═C**H**–). Elemental analysis of MN_NH$_2$: C 40.52.20%, H 6.67%, N 0.69%, S 0.89%. ^{1}H-NMR of MN_POX_NH$_2$ (600 MHz, DMSO), δ (ppm): 1.95 (–C**H**$_3$, POX), 2.66 (–S–CH_2–C**H**$_2$–NH_2), 2.8 (–S–C**H**$_2$–CH_2–NH_2), 3.3–4.3 (–C**H**$_2$–C**H**–, mannose; –N–C**H**$_2$–C**H**$_2$–, POX), 4.97–5.22 (–O–C**H**–O, acetal). Elemental analysis of MN_POX_NH$_2$: C 53.20%, H 8.35%, N 5.2%, S 1.83%.

Conjugation of IR800CW-NHS-ester and DOTA-NHS-ester with the primary amino groups contained in MN_NH$_2$ or MN_POX_NH$_2$ (synthesis of MN_IR_DOTA or MN_POX_IR_DOTA). MN_NH$_2$ or MN_POX_NH$_2$ (454.8 mg, 0.107 mmol of –NH_2 groups or 629.5 mg, 0.123 mmol of –NH_2 groups, respectively), Na_2HPO_4 $12H_2O$ (4.674 g, 13.05 mmol or 6.541 g, 18.26 mmol for MN_NH$_2$ and MN_POX_NH$_2$, respectively) and KH_2PO_4 (293.5 mg, 2.16 mmol or 413 mg, 3.035 mmol for MN_NH$_2$ and MN_POX_NH$_2$, respectively) were dissolved in 32 mL or 42 mL of water (for MN_NH$_2$ and MN_POX_NH$_2$, respectively) and cooled down to 0 °C. A weighted amount of IR800CW-NHS-ester was added (1.8 mg, 0.001545 mmol or 2 mg, 0.00172 mmol for MN_NH$_2$ and MN_POX_NH$_2$, respectively). The reaction mixtures were stirred for 3 h at room temperature. DOTA-NHS-ester (75 mg, 0.0985 mmol or 150 mg, 0.1969 mmol for MN_NH$_2$ and MN_POX_NH$_2$, respectively) was added, and the reaction mixtures were stirred overnight at room temperature. The crude products were purified on a Sephadex® G-25 column using water as the mobile phase and freeze-dried to afford the products MN_IR_DOTA and MN_POX_IR_DOTA (437 mg and 629.5 mg, respectively).

^{1}H-NMR of MN_IR_DOTA (600 MHz, DMSO), δ (ppm): 2.51 (–S–CH_2–C**H**$_2$–NH_2), 2.65 (–S–C**H**$_2$–CH_2–NH_2), 3.4–4.2 (–C**H**$_2$–C**H**–, mannose), 4.7–5.2 (–O–C**H**–O, acetal). ^{1}H-NMR of MN_POX_IR_DOTA (600 MHz, DMSO), δ (ppm): 1.15 (–CH_3, POX), 2.58 (–S–CH_2–C**H**$_2$–NH_2), 2.7 (–S–C**H**$_2$–CH_2–NH_2), 3.4–4.2 (–C**H**$_2$–C**H**–, mannose; –N–C**H**$_2$–C**H**$_2$–, POX), 4.95–5.2 (–O–C**H**–O, acetal).

Finally, MN_IR_DOTA or MN_POX_IR_DOTA was chelated with Gd(III) according to the following procedure: the MN-based conjugate (402 mg or 620 mg for MN_IR_DOTA and MN_POX_IR_DOTA, respectively), ammonium acetate (1.171 g, 15.19 mmol or 1.868 g, 24.23 mmol for MN_IR_DOTA and MN_POX_IR_DOTA, respectively) and gadolinium(III) chloride (171.5 mg, 0.651 mmol or 270 mg, 1.024 mmol for MN_IR_DOTA and MN_POX_IR_DOTA, respectively) were dissolved in water (30 mL or 50 mL for MN_IR_DOTA and MN_POX_IR_DOTA, respectively), and the reaction mixture was stirred overnight at room temperature. The crude products were twice purified on a Sephadex® G-25 column using water as the mobile phase and freeze-dried to provide MN_IR_DOTA-Gd and MN_POX_IR_DOTA-Gd (342 mg and 533 mg, respectively). The content of Gd(III) was determined by energy-dispersive X-ray spectroscopy (EDS) and was found to be 3.94% (0.252 mmol g^{-1}) and 4.22% (0.27 mmol g^{-1}) for MN_IR_DOTA and MN_POX_IR_DOTA-Gd, respectively.

The amount of the IR800CW label was determined spectrophotometrically (0.1 wt%, λ = 774 nm, ε = 240 000 L mol^{-1} cm^{-1}) and was found to be 0.72 μmol and 0.66 μmol for MN_IR_DOTA and MN_POX_IR_DOTA-Gd, respectively.

Characterization

^{1}H NMR measurements were conducted on a Bruker Avance DPX-300 spectrometer operating at 300.13 MHz and on a

Bruker Avance III 600 spectrometer operating at 600 MHz (both Bruker Co., Austria). Fourier transform infrared (FT-IR) spectra were obtained on a Perkin-Elmer Paragon 1000PC spectrometer (Perkin-Elmer Co., USA) equipped with a Specac MKII Golden Gate single attenuated total reflection (ATR) system (Perkin-Elmer Co., USA). Elemental analysis was performed on a Perkin-Elmer Series II CHNS/O Analyzer 2400 (PE Systems Ltd, Czech Republic) instrument. UV-Vis absorption spectra of the obtained conjugates were acquired at a 1 mg mL^{-1} concentration (in phosphate buffered saline, PBS) using a Specord® 250 Plus UV-Vis spectrometer (Jena, Germany) (Fig. SI-1, ESI†). Fluorescence spectra of the samples were recorded (90° angle geometry, 1 × 1 cm quartz cell) at a concentration of 1 mg mL^{-1} (in PBS) using an FP-6200 spectrofluorometer (Jasco Europe, Italy) with an excitation wavelength of 774 nm (Fig. SI-2, ESI†).

The molecular weight of POX was determined using MALDI. The MALDI-TOF mass spectra were acquired with an Ultraflex (Bruker Daltonics, Bremen, Germany) in positive ion reflection mode using delayed extraction. The spectra were taken as the sum of 30 000 shots with a DPSS Nd:YAG laser (355 nm, 1000 Hz). External calibration was used. The specimens were prepared by the dried droplet method. The sample solution (10 mg mL^{-1}), DHB (2,5-dihydroxybenzoic acid; 20 mg mL^{-1}) used as the matrix and sodium trifluoroacetate ($NaCF_3COO$; 10 mg mL^{-1}) as a cationization agent in methanol were mixed at a volume ratio of 4 : 20 : 1.1 μL, and the mixture was deposited on the ground-steel target plate. The drop was dried under ambient atmosphere. The molecular weight of the prepared MN-based polymers was determined by SEC; the system contains a Deltachrom SDS030 pump (Watrex Co., Prague, Czech Republic), a MIDAS autosampler (Spark HOLLAND B.V., Netherlands), a column (STR SEC-100, 5 μm) and a DAWN® HELEOS® multi-angle static light scattering detector (Wyatt Technology Corporation, USA) with acetate buffer used as the mobile phase.

The behaviour of the prepared conjugates in water was studied using dynamic light scattering (DLS) and electrophoretic mobility to determine their hydrodynamic radius (R_{hyd}) and ζ-potential (ZP), respectively. The measurements were conducted on a Zetasizer Nano-ZS, Model ZEN3600 (Malvern Instruments, UK), at a scattering angle $\theta = 173°$ at 25 °C (using DTS software – version 6.20 for data evaluation); data from the volume distribution function were used to determine the hydrodynamic radius R_{hyd}.

Cell viability assay

The cytotoxicity profile of the MN-based conjugates was evaluated using macrophages isolated from the ascites of mice with Abelson murine leukaemia virus-induced tumours (RAW 264.7), macrophages isolated from the ascites of mice with reticulum cell sarcoma (J774A.1), human breast cancer cells from the mammary gland (4T1) and human adenocarcinoma cells from the mammary gland (MCF7) by an Alamar Blue assay. The RAW 264.7 and J774A.1 cell lines were purchased from Merck Ltd (Czech Republic), and the 4T1 and MCF7 cell lines were purchased from LGC Standard Sp.z.o.o. (Poland). The cells were seeded in 96-well flat-bottom plates at concentrations of 8×10^3 cells per well for the RAW 264.7 and J774A.1 cell lines and 5×10^3 cells per well for the 4T1 and MCF7 cell lines in 100 μL of cultivation media at 24 h before adding the polymer conjugates. The cells were incubated at 37 °C in 5% CO_2 with 2 different MN-based conjugates over an equivalent concentration range of 0.004–0.5 mg mL^{-1} for 72 h. Cell viability was measured using Alamar Blue cell viability assay reagent (Thermo Fischer Scientific, Czech Republic). Non-treated cells were used as a viability control (100% viability). The experiment was performed three times in triplicates.

In vitro studies

To characterize the imaging properties of the probes, MN_IR_DOTA-Gd, MN_POX_IR_DOTA-Gd and gadoterate meglumine (GM) were dissolved in distilled water to obtain the same Gd^{3+} concentration (0.36, 0.24, 0.18, 0.12, 0.06, 0.03 mmol L^{-1}) or IR800 dye concentration (1.13, 0.75, 0.56, 0.28, 0.14, 0.07 μg mL^{-1}) for magnetic resonance (MR) and fluorescence (FL) imaging, respectively. The MR properties of the probes were assessed on a 0.5 T Minispec NMR relaxometer (Bruker BioSpin, Germany) by r_1 (saturation recovery sequence, recycle delay of 12 s or 5 s) and r_2 relaxometry (Carr–Purcell–Meiboom–Gill (CPMG) sequence, recycle delay of 10 s, interpulse delay of 1 ms, 5000 points).

MRI was performed on a 4.7 T Bruker Biospec scanner using a resonator coil (Bruker, BioSpin, Germany). T_1-Weighted images were acquired by a turbo spin echo sequence with the following parameters: repetition time TR = 125 ms, echo time TE = 11 ms, turbo factor TF = 2, spatial resolution = 0.27 × 0.27 × 1.5 mm^3, scan time = 6.5 min and fluorescence imaging (10 s of exposure, excitation of 745 nm, and emission of 810–875 nm). Regions of interest (ROIs) were manually outlined around each sample in the MR and FL images, and the signal intensity was assessed. Contrast-to-noise ratio (CNR) values from the MR images were calculated as the difference between the signal intensity from the sample and the water signal intensity (normalized to the water signal). The average FL radiance efficiency was assessed from ROIs covering the samples in the FL images using Living Image software (Perkin-Elmer, USA).

In vivo experiments

The animal experiments described below were performed in the accordance with The Law of Animal Protection against Cruelty (Act No. 359/2012) of the Czech Republic, which is fully compatible with the European Communities Council Directive 86/609/EEC.

For 3 weeks of monitoring *in vivo*, 100 μL of MN_IR_DOTA-Gd or MN_POX_IR_DOTA-Gd (both at concentration of 3.5 mg of Gd^{3+} per mL and 0.64 mg mL^{-1} of IR800 dye) were administered into the calf muscle of the right hind leg of healthy C57/6J B6 mice (n = 3 for each group). MRI was performed on a 4.7 T MR Bruker Biospec scanner (Bruker BioSpin, Germany) using a homemade surface coil. T_1-Weighted axial and coronal MR images of the calf muscles and LNs of mice were acquired using a turbo spin echo sequence with the following parameters: TR= 339 ms, TE = 12 ms, TF = 2, spatial resolution

was = 0.16 × 0.16 × 0.70 mm, 9 slices and scan time = 8 min 40 s. *In vivo* FL images were acquired within a 60 s exposure time using an excitation wavelength at 745 nm and an emission wavelength at 810–875 nm. MRI was performed immediately after agent injection and then at 6 h and 1, 2, 3, 4, 7, 14 and 21 days after contrast agent administration. FLI was conducted at the same time points as MRI and before and 2 h after agent administration. One animal per group was sacrificed at days 7, 14 and 21, and its internal organs were excised and subjected to *ex vivo* FLI.

CNR values of the inguinal LNs were calculated in percentage from the MR images as the difference between the signal intensities of the LN and the surrounding fat (normalized to the fat signal) to suppress inhomogeneity originating from the surface coil. FL was evaluated from *in vivo* images of the liver and the lymph nodes and from *ex vivo* images of excised organs (spleen, liver, kidney, and inguinal LNs).

Results and discussion

The natural biodegradable polysaccharide MN was modified in two different ways to obtain conjugates bearing a fluorescent label and a probe for MRI. The first approach was focused on the synthesis of a polysaccharide-based conjugate without polyoxazoline in the structure (Scheme 2A). The modification procedure began with the alkylation of commercial MN (from *S. cerevisiae*) with allyl bromide in alkaline aqueous solution to

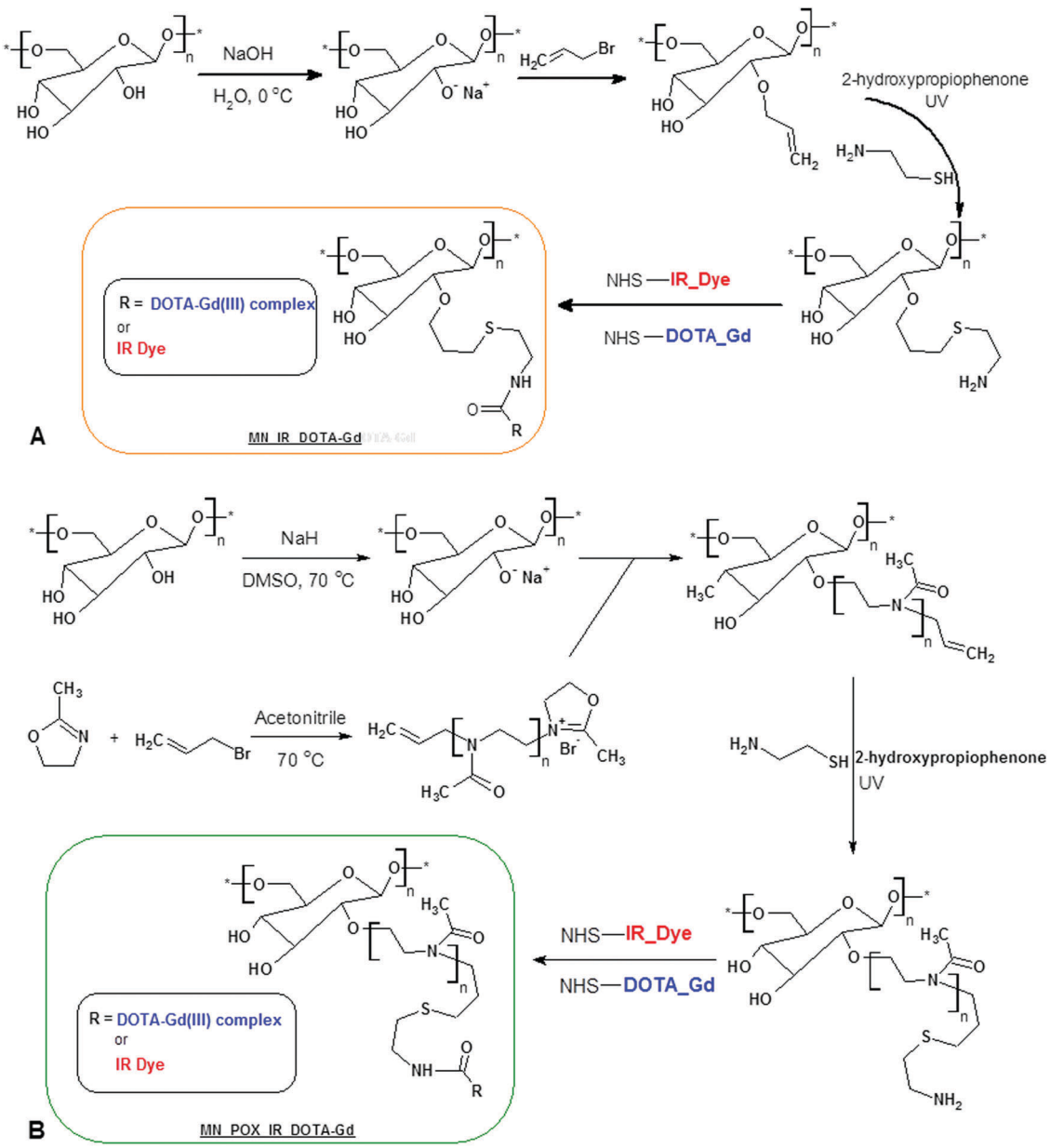

Scheme 2 Synthetic route for mannan modification: preparation of MN_IR_DOTA-Gd (A) and MN_POX_IR_DOTA-Gd (B).

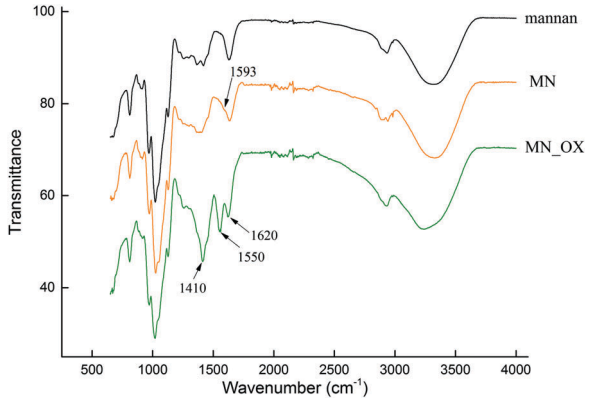

Fig. 1 FTIR spectra of native mannan (black line), MN_IR_DOTA-Gd (orange line) and MN_POX_IR_DOTA-GD (dark green line).

obtain the vinyl-containing derivative of MN (MN_allyl, 12.66 mol% of allyl). This derivative was later reacted with cysteamine using 2-hydroxy-2-methylpropiophenone as initiator under UV irradiation. This primary amino group-containing MN was then conjugated with *N*-hydroxysuccinimide (NHS) esters of an infrared dye (IR800CW NHS-ester) and 1,4,7,10-tetraazacyclododecane-1,4,7,10-tetraacetic acid (DOTA NHS-ester). Finally, the obtained product was reacted with gadolinium(III) chloride to chelate Gd^{3+}, resulting in an MN-based conjugate with FL and MR imaging labels, denoted MN_IR_DOTA-Gd.

Grafting with a synthetic polymer decreases the biodegradation rate[44,45] of the polysaccharide and introduces the possibility of easy functionalization of the ends of the polymer grafts with active cargo. The synthetic approach for the preparation of MN-based conjugate with grafted polyoxazoline chains was slightly different from that for MN_IR_DOTA-Gd (Scheme 2B). After dissolution in anhydrous DMSO, MN sodium alkoxide was reacted with active POX chains obtained by ring-opening cationic polymerization in anhydrous acetonitrile. Different MN grafting

Table 1 Characteristics of native and modified mannan

Name	$M_w \times 10^3$,[b] g mol^{-1}	R_{hyd},[c] nm		ZP,[c] mV	
		H_2O	PBS	H_2O	PBS
Mannan[a]	44.6	1.2	3.6	0.2	−5.6
MN_IR_DOTA-Gd	52	3.1	3.3	−4.0	−11.5
MN_POX_IR_DOTA-Gd	71.2	3.0	3.6	2.9	−6.7

[a] Commercial (native) mannan from *Saccharomyces cerevisiae*. [b] Determined by mass spectrometry. [c] Obtained from dynamic light scattering and electrophoretic mobility measurements.

reactions with POX were performed (data not shown) to determine the maximal achievable grafting density, which was found to be 30 mol%. Consequently, mannan-*graft*-poly(2-methyl-2-oxazoline) (denoted MN_POX) with a grafting density of 1 graft per 5 glucose units (29.73 mol% of POX from ^{1}H NMR) was selected for this work. The molecular weight of POX grafts was determined by mass spectrometry after termination of active chains with water: number-average molecular weight M_n = 870 g mol^{-1}, polydispersity PDI = M_w/M_n = 1.14, where M_w is the weight-average molecular weight.

Because the starting MN from *S. cerevisiae* contained less than 0.3 wt% nitrogen, the weight content of POX in the prepared polymers could be calculated from elemental analysis (CHN) according to the following equation:

$$w_{pMeOx} = \frac{w_N}{w_{N,pMeOx}} \times 100\%$$

where w_N is the content of nitrogen in the sample (determined by CHN elemental analysis) and $w_{N,PMeOx}$ is the calculated content of nitrogen in the POX graft (16.45% in our case). The POX content for MN_POX was found to be 19.94 wt%.

Next, allyl-containing mannan derivatives were modified by radically initiated thiol–ene click chemistry with cysteamine to obtain conjugates with primary amino groups (Scheme 2B). These primary amino groups then can be easily modified with

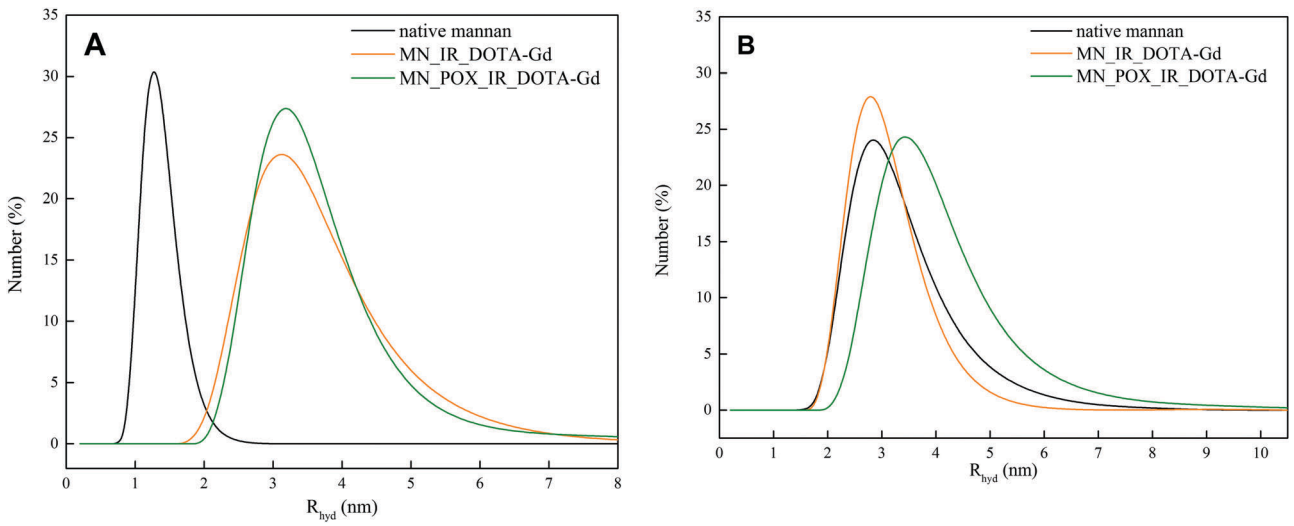

Fig. 2 Dynamic light scattering results of native mannan from *Saccharomyces cerevisiae* and of the mannan-based conjugates in water (A) and PBS (pH = 7.4) (B) at a concentration of 1 mg mL^{-1}.

fluorescence- and/or MRI-active labels. For this purpose, the amino-functionalized polysaccharides were reacted with the NHS ester of IR800CW dye as infrared (IR) active fluorescence label and the NHS ester of an MRI T_1 contrast agent – Gd^{3+}-DOTA (Scheme 2B).

Both of the resulting mannan-based conjugates – those without and with POX chains in the structure, MN_IR_DOTA-Gd and MN_POX_IR_DOTA-Gd, respectively – were twice purified on a Sephadex G-25® column using water as the eluent, and then their aqueous solutions were lyophilized. The content of IR dye was determined spectrophotometrically in water (λ = 774 nm, ε = 240 000 M^{-1} cm^{-1}) and was found to be 0.72 and 0.66 μmol g^{-1} in the MN_IR_DOTA-Gd and MN_POX_IR_DOTA-Gd conjugates, respectively. The content of gadolinium in the final products was determined by inductively coupled plasma mass spectrometry and was found to be 0.252 and 0.26 mmol g^{-1} for MN_IR_DOTA-Gd and MN_POX_IR_DOTA-Gd, respectively. The obtained concentrations of Gd^{3+} in the prepared mannan probes correspond to 13 and 19 gadolinium atoms per molecule of MN_IR_DOTA-Gd and MN_POX_IR_DOTA-Gd, respectively.

Fourier transform infrared (FTIR) spectroscopy was used to prove the bonding of the IR and DOTA labels to both MN derivatives. The IR spectrum of neat MN shows peaks at 3320, 2934, 1635 and 1022 cm^{-1}, which correspond to ν(OH), $\nu_{as}(CH_2)$, ν(CO) and ν(COC) vibrations, respectively (Fig. 1). Because the MN used was extracted from baker's yeast, we attribute the appearance of carbonyl groups in the spectrum to the presence of a small amount of peptide residues in its structure. The FTIR spectrum of MN_IR_DOTA-Gd exhibits the appearance of a weak δ(NH) deformation vibration peak located at 1593 cm^{-1}, confirming the successful bonding of the IR and DOTA labels through amide groups. For the MN_POX_IR_DOTA-Gd conjugate, this peak is probably overlapped by strong ν(CO) vibrations at 1620 and 1550 cm^{-1} originating from the grafted POX chains.

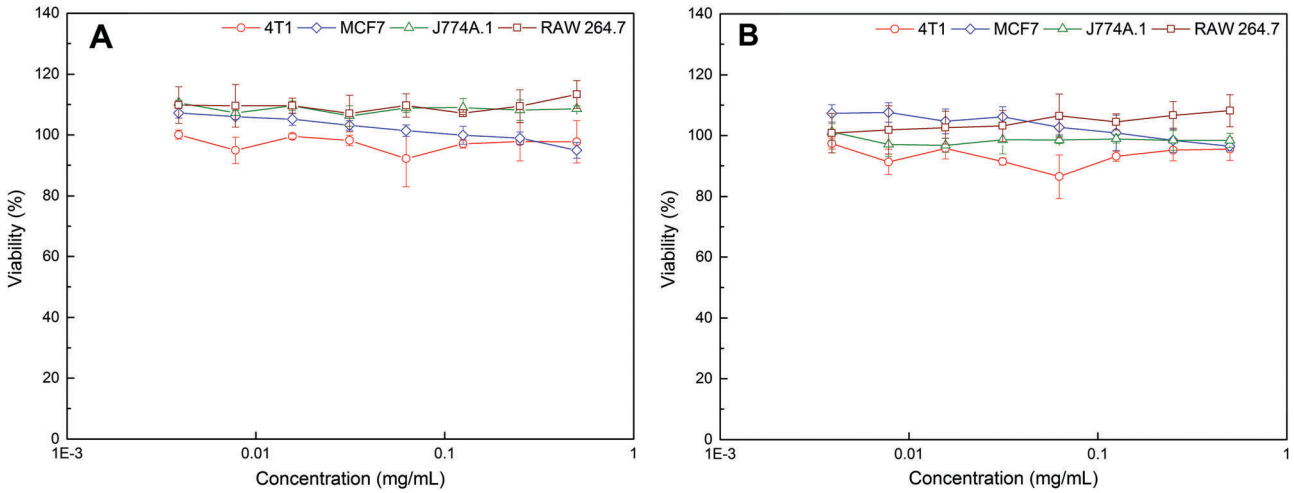

Fig. 3 Viability of MN_IR_DOTA-Gd (A) and MN_POX_IR_DOTA-Gd (B) in macrophage (RAW 264.7 and J774A.1) and mammary gland (4T1 and MCF7) cell lines as a function of conjugate concentration (0.004–0.5 mg mL^{-1}) after 72 h of incubation at 37 °C in 5% CO_2. Treated cells were compared to controls (without addition of MN-based conjugates) to obtain percent viability.

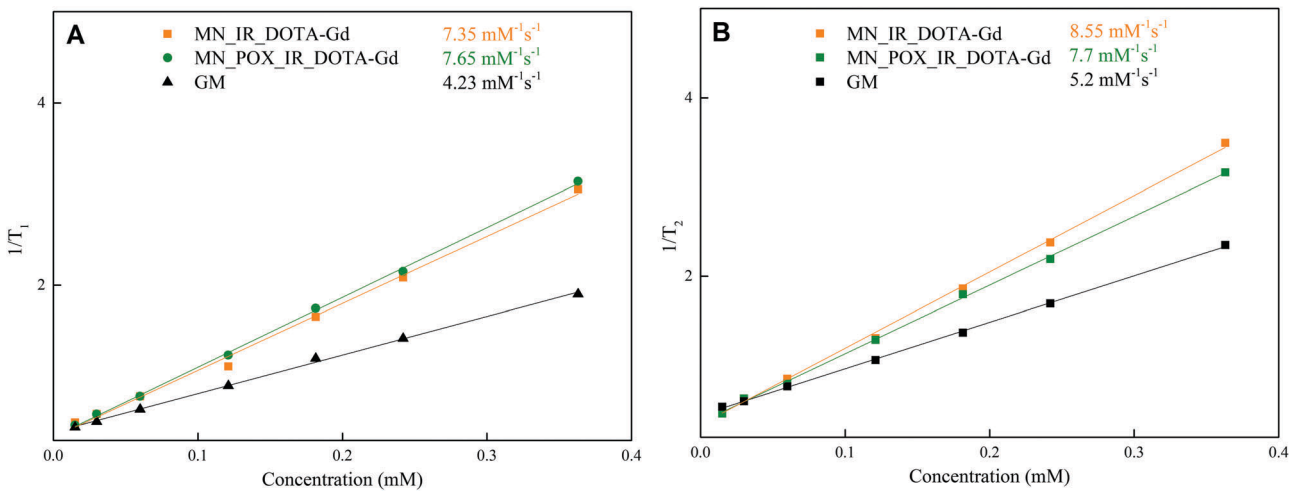

Fig. 4 Characterization of the probes – ^1H r_1 (A) and r_2 (B) relaxivities of the tested probes measured at 0.5 T (25 °C).

Another conformation of the successful grafting of MN with the POX chains is the appearance of a strong ν(C=C) vibration at 1410 cm^{-1} of the vinyl end group of POX.

To characterize the behaviour of the prepared conjugates in aqueous solution, dynamic light scattering (DLS) measurements were conducted using a Zetasizer Nano-ZS (Malvern) instrument. To determine the difference in hydrodynamic diameter due to the modification procedure, native MN from *S. cerevisiae* and both of the prepared conjugates were dissolved in Q-water or phosphate buffered saline (PBS) at a concentration of 1 mg mL^{-1}, and DLS measurements were performed (Fig. 2).

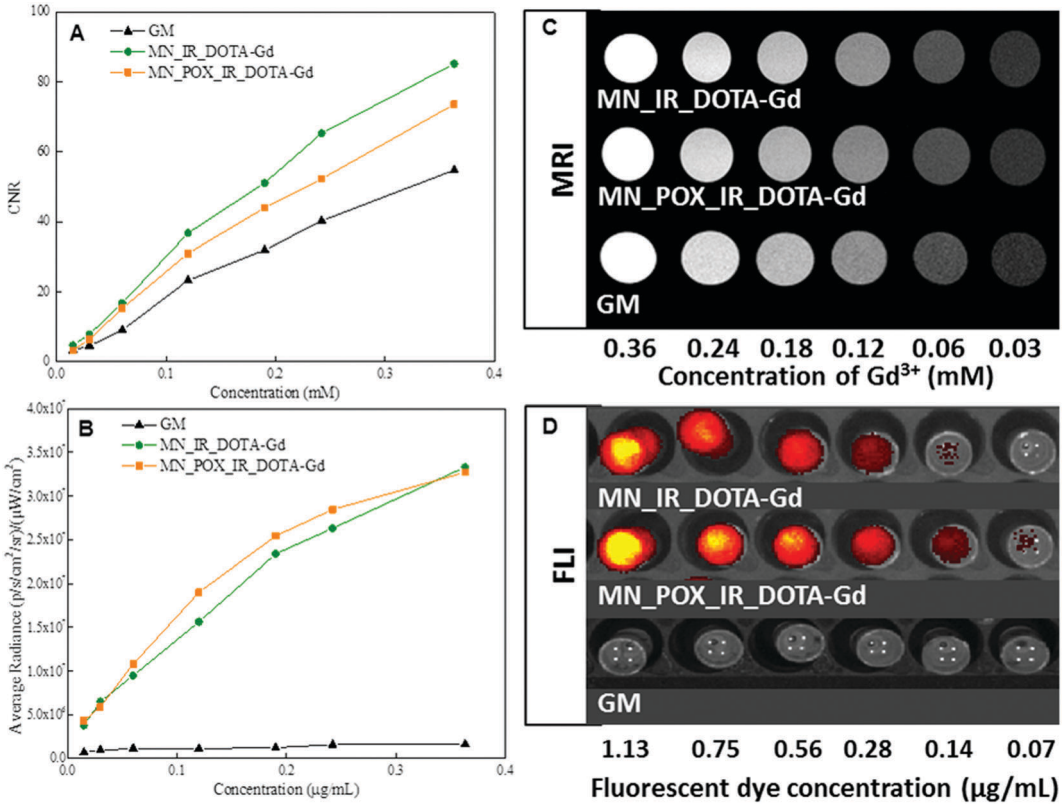

Fig. 5 The magnetic resonance (MR) and fluorescence (FL) signals of the MN_IR_DOTA-Gd, MN_POX_IR_DOTA-Gd and gadoterate meglumine (GM). Contrast-to-noise ratio (CNR) was calculated from the MR images (A) and FL signal (B) of the probes at various concentration of Gd^{3+} or fluorescent dye. Representative MR images of the probes with different Gd^{3+} concentrations (C) – the numbers represent Gd^{3+} concentration expressed in mM; the FL images of the probes with different dye concentrations (D); the numbers represent the concentration of fluorescent dye expressed in μg mL^{-1}.

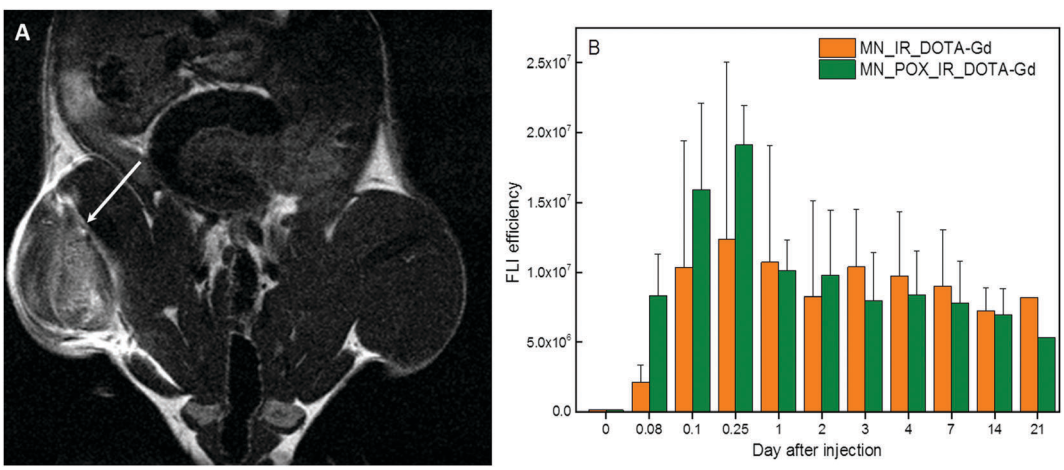

Fig. 6 Representative T_1-weighted magnetic resonance (MR) image of a mouse injected in its hind leg with the MN_IR_DOTA-Gd probe (A); the arrow denotes the injection site. The time course of the fluorescence (FL) signal from the injection site (muscle) (B).

Fig. 2 presents the size distributions of the neat and modified MN in water and in PBS. Because of the modification procedure described above, the hydrodynamic radius of MN was found to increase. In aqueous solution, the R_{hyd} of both MN_IR_DOTA-Gd and MN_POX_IR_DOTA-Gd were *ca.* two times larger ($\sim$3 nm) than native MN (1.2 nm). In comparison to that of native MN, the ζ-potential (ZP) of MN_IR_DOTA-Gd decreased to -4 mV (Table 1), confirming the presence of ionic carboxylate groups from the FLI and MRI contrast labels. In the case of MN_POX_IR_DOTA-Gd, the ZP had increased to 2.9 mV, indicating the presence of grafted POX chains in its structure. When PBS was used as solvent (pH = 7.4), no significant difference in hydrodynamic radius could be observed between native MN and the modified MN derivatives ($R_{hyd} \sim 3.5$ nm). In contrast to aqueous solution, the ZP values in PBS (pH = 7.4) of all three samples were small and negative, probably due to formation of a counter ion layer (Table 1). Moreover, the DLS measurements performed in water at different pH ranging from 5 to 9 did not show a significant change in hydrodynamic radius of either of the prepared MN-based probes (R_{hyd} from 2 to 4 nm). Those results show that the behaviour of the prepared conjugates is insensitive to different pH or increased ionic strength, which is beneficial for the intended application.

To study the biocompatibility of the synthesized MN-based conjugates, *in vitro* testing with four different cell lines was conducted. As shown in Fig. 3, no significant changes in the viabilities of any of the treated cells were observed after incubation with the prepared conjugates. The viability varied within the experimental error between 85 and 110% of the control (non-treated cells). There were no concentration-dependent changes in the cytotoxicity of the conjugates. The obtained results prove the potential of the new MN derivatives for use in biomedical applications, for instance as a drug delivery system targeted to immune and metastatic cells or as a diagnostic probe with enhanced tumour accumulation and specific targeting for LNs.

To demonstrate the imaging performance of the prepared conjugates, an *in vitro* experiment on phantoms was performed first. Both MN-based agents showed higher r_1 and r_2 relaxivities than commercially available GM (Fig. 4A and B) based on Gd^{3+} concentration, probably due to the decreased mobility of the chelated gadolinium arising from the conjugation to relatively high-molecular-weight polymers. On the other hand, the relaxivities of MN_IR_DOTA-Gd and MN_POX_IR_DOTA-Gd were comparable. Similarly, the MR signals and corresponding contrast-to-noise ratio (CNR) values of the MN-based probes were higher than those of GM (Fig. 5A and C).

The MN-based agents also showed a strong FL signal, whereas the FL of GM was in the range of the background as expected (Fig. 5B and D). Therefore, these promising *in vitro* results encouraged us to perform pilot *in vivo* experiments on healthy mice. GM is not fluorescent and is not an actively LN-targeted probe; thus, only MN-based contrast agents are discussed hereinafter for the *in vivo* experiments.

After intramuscular administration to the mice, both the MN_IR_DOTA-Gd and MN_POX_IR_DOTA-Gd agents were visualized at the injection sites by MRI and FLI for 21 days. The 21-day imaging was performed to monitor the *in vivo* fate

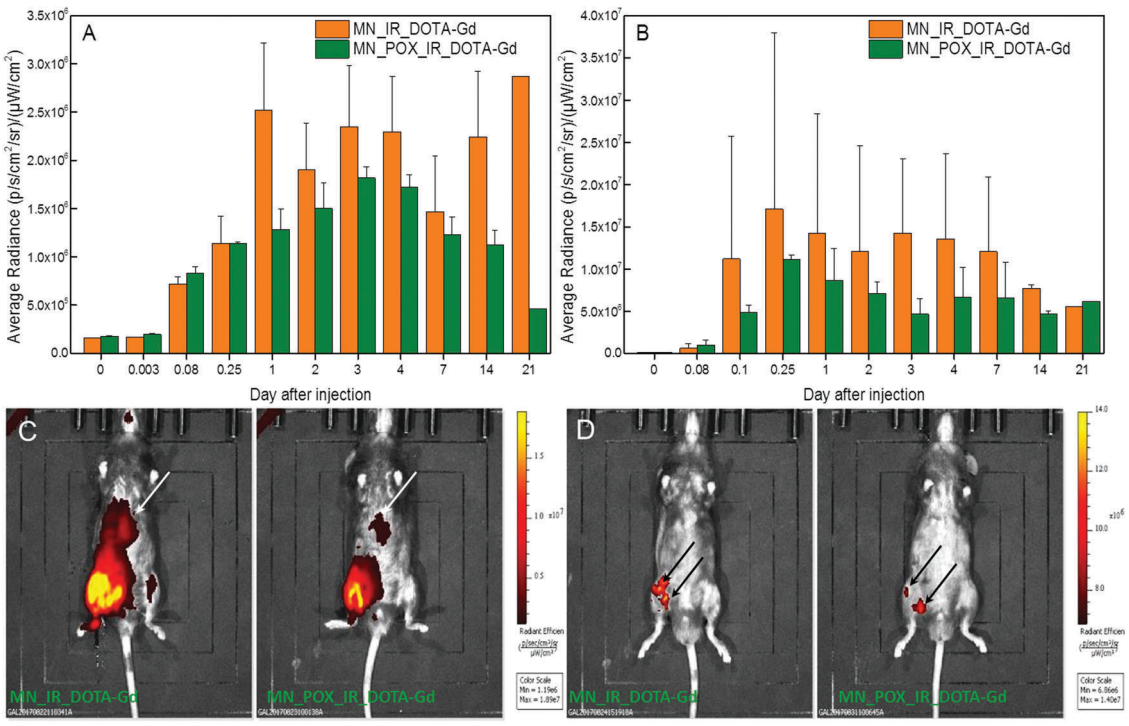

Fig. 7 Time course of the *in vivo* fluorescence (FL) signal originating from the liver (A) and the lymph nodes (B). Representative fluorescence images of mice after injection with MN_IR_DOTA-Gd and MN_POX_IR_DOTA-Gd (C and D). The arrows denote the liver (C) and the lymph nodes (D).

and biodegradability of the conjugates and to find the optimal time for the highest contrast against the surrounding tissues. The FL signal increased within the first day and then continuously decreased until the end of the examination. The most plausible explanation for this effect is that immediately after administration, the contrast agent is concentrated within a small volume, and because of the high concentration, it self-quenches. Over time, the contrast agent spreads to a larger volume (and the emitting area exposed to the detector is therefore larger). Thus, the quenching effect is no longer as prominent, and as a result, paradoxically, more photons capable of penetrating through the skin, are detected. Fig. 6B shows that the fluorescence signal of MN_POX_IR_DOTA-Gd in muscle was higher than that of MN_IR_DOTA-Gd within the first two days after injection, demonstrating that POX grafting prolonged the imaging window and that biodegradation of the conjugate was slower.

Moreover, the FL signal was visualized in the liver site after injecting the probes. After 1 day, the FL signal originating from MN_IR_DOTA-Gd was higher than that originating from MN_POX_IR_DOTA-Gd, and this trend persisted to the end of the examination time (Fig. 7A and C). Within the first day after probe administration, higher FL and MR signals from the LNs were detected in case of MN_IR_DOTA-Gd, confirming its faster degradation (Fig. 7B, D and 8).

MRI confirmed the presence of the injected probes at the muscle sites (Fig. 6A) and in the LNs of both mice (*i.e.*, those treated with MN_IR_DOTA-Gd and MN_POX_IR_DOTA-Gd) (Fig. 8B). Within the first day after probe administration, the MR signal of MN_IR_DOTA-Gd was higher than that of MN_POX_IR_DOTA-Gd, which in agreement with the results obtained from FLI. As seen in Fig. 6B and 7B, which present the time courses of the FL signal originating from injected site and LNs, respectively, the signals were similar, with an average value of 1.5×10^7. The MR signal in the non-injected muscle (*i.e.*, background; see Fig. 6A) was much lower, which is important for the intended use, and the evaluated MR signal data from the LNs (Fig. 8A) clearly show the stable presence of the contrast agents.

In addition, e*x vivo* FLI of the harvested organs also confirmed the lower accumulation of MN_POX_IR_DOTA-Gd in the liver, spleen and kidneys for all time intervals (7, 14, and 21 days) (Fig. 9). The signals originating from the LNs were comparable for both the MN_IR_DOTA-Gd and MN_POX_IR_DOTA-Gd conjugates within 7, 14 and 21 days after probe administration (Fig. 9J–L). Although the FL signal

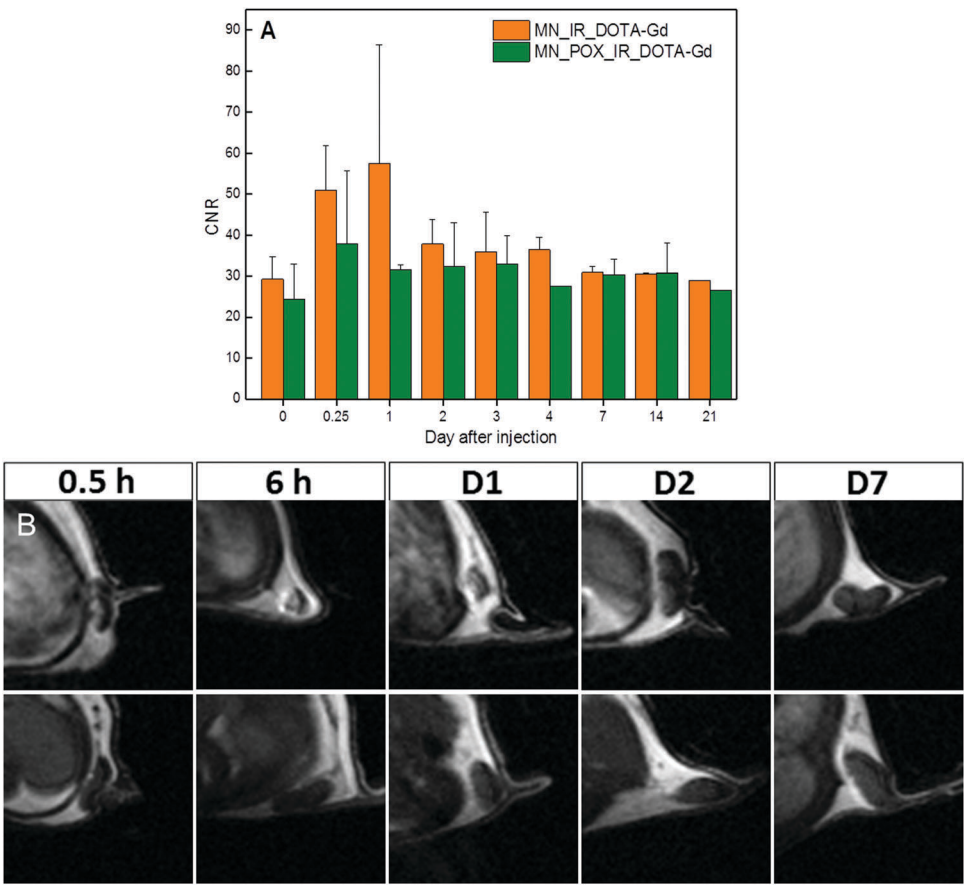

Fig. 8 Time course of the magnetic resonance (MR) signal in the lymph nodes of mice after injection with MN_IR_DOTA-Gd or MN_POX_IR_DOTA-Gd (A). Representative T_1-weighted MR images show the lymph nodes at different time points (B) after MN_IR_DOTA-Gd (top) or MN_POX_IR_DOTA-Gd (bottom) administration.

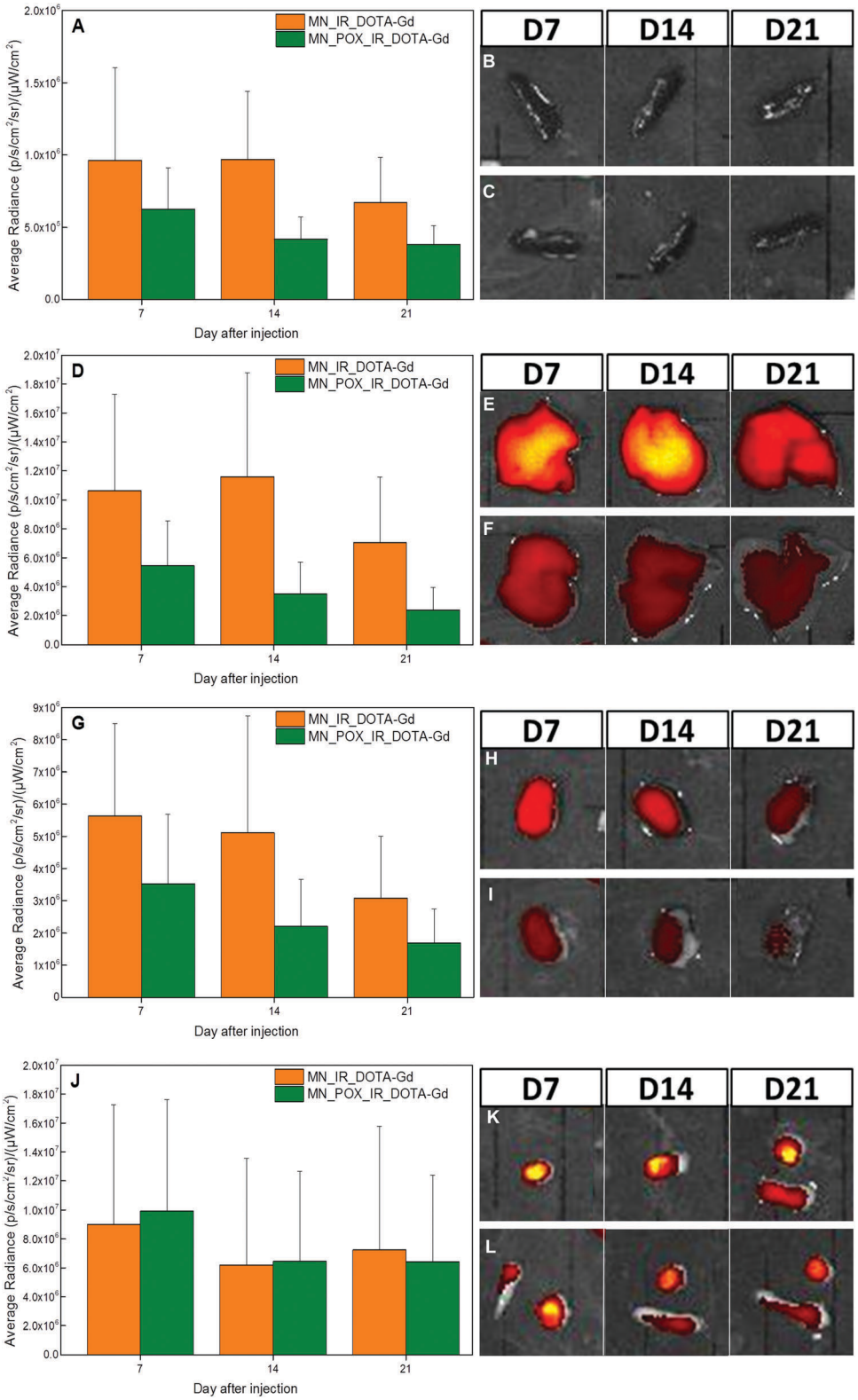

Fig. 9 Average radiant efficiency in the spleen (A), liver (D), kidney (G) and lymph nodes (J) *ex vivo*. Fluorescence (FL) signal after 7, 14 and 21 days from the spleen (B and C), liver (E and F), kidney (H and I) and lymph nodes (K and L) after administration of MN_IR_DOTA-Gd (B, E, H and K) or MN_POX_IR_DOTA-Gd (C, F, I and L).

from the LNs remained very similar throughout whole examination time, the signal from organs (liver, spleen, kidneys) continuously decreased over time for both conjugates, indicating the gradual biodegradation of the MN probes.

Therefore, the novel MN-based compounds possess superior properties compared to the commercially available contrast agent GM, including their MR relaxivity and FLI capability. The visualized accumulation of the agents in the LNs confirmed their immune system-targeted properties and possible use in metastasis diagnostics.

Conclusions

We demonstrated an easy synthetic approach for preparing novel multimodal MN-based probes intended for immune cell detection. The obtained conjugates contained both a fluorescent IR dye and a Gd^{3+} MRI contrast agent in their structures. The content of the FL label was estimated spectrophotometrically and was found to be 0.72 and 0.66 μmol g^{-1} for MN_IR_DOTA-Gd and MN_POX_IR_DOTA-Gd, respectively. The chelation efficiency of DOTA with Gd^{3+} was analysed by inductively coupled plasma mass spectrometry, and the concentration of Gd^{3+} in MN_IR_DOTA-Gd and MN_POX_IR_DOTA-Gd was 0.252 and 0.26 mmol g^{-1}, respectively. The prepared probes possessed sufficient sensitivity for *in vivo* FLI and exhibited superior MRI properties compared to a commercial contrast agent. The MN-based conjugates were detected in organs 3 weeks after probe administration, indicating their slow biodegradation; however, the strongest MRI and FLI signals were detected within the first day following agent administration. Moreover, the appearance of a lower FL signal at the liver and higher FL signal at the administrated site in the mouse injected with MN_POX_IR_DOTA-Gd suggested its slower elimination process due to the addition of POX chains in its structure. The possibility of further chemical modification of the obtained MN-based conjugates for incorporating specific drugs, for obtaining structures with a suitable size for enhanced accumulation in tumours and for achieving specific targeting of LNs makes these agents promising as a drug delivery system targeted to immune and metastasis cells.

Conflicts of interest

There are no conflicts to declare.

Acknowledgements

The authors acknowledge financial support from the Ministry of Health of the Czech Republic (grant # 15-25781a). The authors also acknowledge the Charles University in Prague for the opportunity for doctoral studies provided to M. Rabyk.

References

1 A. Basu, K. R. Kunduru, E. Abtew and A. J. Domb, *Bioconjugate Chem.*, 2015, **26**, 1396.
2 E. Muntimadugu, D. E. Ickowicz, A. J. Domb and W. Khan, *Isr. J. Chem.*, 2013, **53**, 787.
3 S. N. Lakshmi and C. T. Laurencin, *Prog. Polym. Sci.*, 2007, **32**, 762.
4 K. M. Colvin, V. D. Gordon, K. Murakami, B. R. Borlee, D. J. Wozniak, G. C. L. Wong and M. R. Parsek, *PLoS Pathog.*, 2011, **7**(1), e1001264.
5 Z. Liu, Y. Jiao, Y. Wang, C. Zhou and Z. Zhang, *Adv. Drug Delivery Rev.*, 2008, **60**, 1650.
6 Y. Zhang, H. F. Chan and K. W. Leong, *Adv. Drug Delivery Rev.*, 2013, **65**, 104.
7 N. B. Shelke, R. James, C. T. Laurencin and S. G. Kumbar, *Polym. Adv. Technol.*, 2014, **25**, 448.
8 C. Goncalves, S. A. Ferreira, A. L. Correira, C. Lopes, C. E. Fleming, E. Rocha, M. Vilanova and M. Gama, *J. Bioact. Compat. Polym.*, 2016, **31**, 453.
9 T. Azzam, H. Eliyahu, L. Shapira, M. Linial, Y. Barenholz and A. J. Domb, *J. Med. Chem.*, 2002, **45**, 1817.
10 T. Kutlusoy, B. Oktay, N. K. Apohan, M. Suleymanoglu and S. C. Kuruca, *Int. J. Biol. Macromol.*, 2017, **103**, 366.
11 M. Lepore, M. Portaccio, I. Delfino, L. Sironi, A. La Gatta, A. D'Agostino, E. Izzo and C. Schiraldi, *J. Appl. Polym. Sci.*, 2017, **134**, 45243.
12 S. Naahidi, M. Jafari, M. Logan, Y. Wang, Y. Yuan, H. Bae, B. Dixon and P. Chen, *Biotechnol. Adv.*, 2017, **5**, 530.
13 N. P. Birch and J. D. Schiffman, *Langmuir*, 2014, **30**, 3441.
14 N. Goodarzi, R. Varshochian, G. Kamalinia, F. Atyabi and R. Dinarvand, *Carbohydr. Polym.*, 2013, **92**, 1280.
15 A. Shimoda, S. Sawada, A. Kano, A. Maruyama, A. Moquin, F. M. Winnik and K. Akiyoshi, *Colloids Surf., B*, 2012, **99**, 38.
16 Y. Yu, H. Zhang, H. Sun, D. Xing and F. Yao, *Front. Chem. Sci. Eng.*, 2013, **7**, 388.
17 Z. Odabasi, G. Mattiuzzi, E. Estey, H. Kantarjian, F. Saeki, R. J. Ridge, P. A. Ketchum, M. A. Finkelman, R. H. Rex and L. Ostrosky-Zeichner, *Clin. Infect. Dis.*, 2004, **2**, 199.
18 S. Pan, T. A. Brentnall and R. Chen, *World J. Gastroenterol.*, 2016, **22**, 9288.
19 S. B. Majee, D. Avlani and G. R. Biswas, *Afr. J. Pharm. Pharmacol.*, 2017, **11**, 68.
20 A. Martin-Fontecha, A. Lanzavecchia and F. Sallusto, in *Handbook of Experimental Pharmacology*, ed. G. Lombardi and Y. Riffo-Vasquez, Springer-Verlag, Berlin, 2009, vol. 188, pp. 31–49.
21 S. Karaman and M. Detmar, *J. Clin. Invest.*, 2014, **124**, 922.
22 G. H. Lyman, S. Temin, S. B. Edge, L. A. Newman, R. R. Turner, D. L. Weaver, A. B. Benson, L. D. Bosserman, H. J. Burstein, H. Cody, J. Hajman, C. L. Perkins, D. A. Podoloff and A. E. Giuliano, *J. Clin. Oncol.*, 2014, **13**, 1365.
23 P. Szychta, B. Westfal, R. Maciejczyk, B. Smolarz, H. Romanowicz, T. Krawczyk and M. Zadrozny, *Arch. Med. Sci.*, 2014, **12**, 1239.
24 S. M. Ha, J. H. Cha, H. H. Kim, H. J. Shin, E. Y. Chae and W. J. Choi, *Acta Radiol.*, 2017, **10**, 1198.
25 J. P. Hoogendam, R. P. Zweemer, M. G. G. Hobbelink, M. A. A. J. van den Bosch, R. M. H. Verheijen and W. B. Veldhuis, *J. Nucl. Med.*, 2016, **4**, 551.
26 P. T. Soliman, S. N. Westin, S. Dioun, C. C. Sun, E. Euscher, M. F. Munsell, N. D. Fleming, C. Levenback, M. Frumovitz, P. T. Ramirez and K. H. Lu, *Gynecol. Oncol.*, 2017, **2**, 234.
27 L. Huang, T. Wei, J. Chen and D. Zhou, *World J. Surg. Oncol.*, 2017, **15**(1), 103.

28 E. A. Newman and L. A. Newman, *Surg. Clin. North Am.*, 2007, **87**, 353.
29 C. Tausch, A. Baege and C. Rageth, *OncoTargets Ther.*, 2014, **7**, 1151.
30 M. J. Stoutjesdijk, C. Boetes, G. J. Jager, L. Beex, P. Bult, J. H. C. L. Hendrik, R. J. F. Laheij, L. Massuger, L. E. Van Die, T. Wobbes and J. O. Barentsz, *J. Natl. Cancer Inst.*, 2001, **93**, 1095.
31 S. K. Shetty and M. G. Harisinghani, *Appl. Radiol.*, 2004, **232**, 897.
32 R. Madru, P. Kjellman, F. Olsson, K. Wingardh, C. Ingvar, F. Stahlberg, J. Olsurd, J. Latt, S. Fredriksson, L. Knutsson and S. E. Strand, *J. Nucl. Med.*, 2012, **53**, 459.
33 R. Ting, T. A. Aguilera, J. L. Crisp, D. J. Hall, W. C. Eckelman, D. R. Vera and R. Y. Tsien, *Bioconjugate Chem.*, 2010, **21**(10), 1811, DOI: 10.1021/bc1001328.
34 M. R. S. Keshtgar and P. J. Ell, *Eur. J. Nucl. Med.*, 1999, **26**, 57.
35 G. Niu and X. Chen, Lymphatic Imaging: Focus on Imaging Probes, *Theranostics*, 2015, **5**(7), 686.
36 M. Yamabhai, S. Sak-Ubol, W. Srilaand and D. Haltrich, *Crit. Rev. Biotechnol.*, 2014, **1**, 32.
37 S. A. Ferreira, P. J. G. Coutinho and F. M. Gama, *Langmuir*, 2010, **26**, 11413.
38 Z. Cui, C. H. Hsu and R. J. Mumper, *Drug Dev. Ind. Pharm.*, 2003, **29**, 689.
39 N. Adams and U. S. Schubert, *Adv. Drug Delivery Rev.*, 2007, **59**, 1504, DOI: 10.1016/j.addr.2007.08.018.
40 H. Schlaad, C. Diehl, A. Gress, M. Meyer, A. L. Demirel, Y. Nur and A. Bertin, *Macromol. Rapid Commun.*, 2010, **31**, 511.
41 R. Hoogenboom and H. Schlaad, *Polymers*, 2011, **3**(1), 468.
42 P. Wilson, P. C. Ke, T. P. Davis and K. Kempe, *Eur. Polym. J.*, 2017, **88**, 486, DOI: 10.1016/j.eurpolymj.2016.09.011..
43 G. T. Hermanson, in *Bioconjugate techniques*, ed. J. Audet and M. Preap, Elsevier Inc., 3rd edn, 2013, vol. 3, pp. 229–258.
44 G. Pitarresi, C. Fiorica, F. S. Palumbo, S. Rigogliuso, G. Ghersi and G. Giammona, *J. Biomed. Mater. Res., Part A*, 2014, **102A**, 1334.
45 X. Xu, A. K. Jha, D. A. Harrington, M. C. Farach-Carson and X. Jia, *Soft Matter*, 2012, **8**, 3280.

